STUDIES OF THE THERMALHYDRAULICS OF THE IRRIADIATION RESEARCH FACILITY (IRF) CHIMNEY USING COMPUTATIONAL FLUID DYNAMICS

T. H. Lan and A. O. Banas
Fuel Channel Thermalhydraulics Branch
Chalk River Laboratories, AECL
Chalk River, Ontario K0J 1J0

1. INTRODUCTION

AECL is developing a concept for a new Irradiation Research Facility (IRF) [1] that will be used to support ongoing development of CANDU technology and advanced materials research after the NRU reactor shuts down. As part of the IRF Pre-Project Engineering Program, computational fluid dynamics (CFD) analyses of the flow patterns and heat transfer within four reactor components—the inlet plenum, reflector tank, chimney, and the pool—were done to support the design. This paper describes the results of the CFD analyses of the IRF chimney.

The IRF reactor structure is submerged in a pool of light water. The design uses up-flow forced-convection cooling to remove the heat produced in the core. The chimney is located above the core and directs the flow from the core back to the primary cooling circuit. A flow is also induced downwards in the chimney, by directing a fraction of the inlet flow to the pool. This downward flow confines the up-flow to the chimney, thereby preventing the escape of the water containing activation products to the pool surface where it would present a radiation hazard. This CFD analysis was conducted to confirm this core jet confinement.

To do these analyses, the commercial CFD package, CFX-4 [2], was used to model the flow and heat transfer inside the chimney. Two grids were generated. Three simulations were performed using these grids and different boundary conditions. The results show that, with the current IRF design, the core jets are contained inside the chimney. Full-scale tests were previously performed for the MAPLE-X10 and HANARO reactors, and test data from the former tests will be used to validate this application of CFX-4.

2. THE IRF CHIMNEY DESIGN

The chimney is an octogonal 2.6-m-high, open-top structure located on the top of the reactor vessel (Figure 1). During normal, pumped-flow operation, the chimney collects the light water exiting the main core and four fast-neutron (FN) fuel sites, and directs it through two outlet pipes back to the primary cooling circuit. The top of the chimney is open to the pool. During reactor shutdown, decay heat from the core is removed by natural circulation of the pool water entering the inlet plenum at the base of the reactor and exiting the top of the chimney.

At steady-state normal operating conditions, about 10% of the primary-circuit cooling flow is branched to the bottom of the pool to by-pass the core, and enter the top of the chimney. This by-pass flow mixes with the remaining 90% of the coolant jetting out of the main core and FN channels, and the mixed stream is discharged through the outlet pipes connected on opposite sides of the chimney. The main core comprises two adjacent segments, each containing twelve 36-element and four 18-element fuel bundles. About 10% of the coolant flow passes through the FN channels and enters the chimney through four openings located on its side walls.

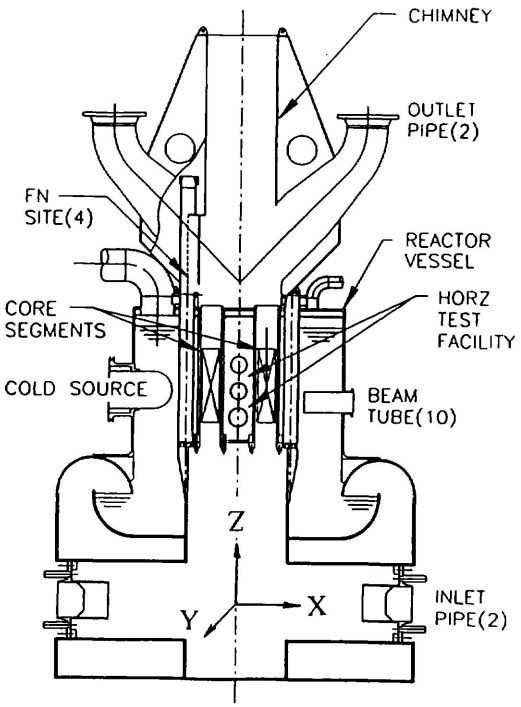

Fig.1 Cutaway of the IRF

The chimney also supports eight control rods, which extend above the core and partially obstruct the chimney exits to the outlet pipes. Each control rod consists of a cylindrical hafnium absorber surrounding an extended flow tube, which in turn surrounds an 18-element fuel bundle. The upper part of the flow tube and the absorber are surrounded by a shroud tube to isolate them from the turbulent flow in the lower part of the chimney.

Under normal operation the downward flow in the chimney confines the water leaving the core to the chimney. This confinement prevents the transport of activation products contained in the water to the pool surface where they would pose a radiation hazard. The CFD analysis of the flow pattern in the chimney, reported in this paper, was performed to confirm the ability of the down flow to suppress any chimney outflow under the specified operating conditions. The analysis provided insight into the factors governing the core jet confinement and confirmed that the present chimney geometry is acceptable.

3. GRID GENERATION

The mathematical formulation of a CFD model of the flow and heat-transfer processes involves two types of discretization. One is the space discretization that divides the geometric model into cells. This discretization is referred to as grid generation. The next stage involves the discretization of the governing partial differential equations. This discretization leads to the transformation of these equations into a set of algebraic equations involving the values of the unknowns at the grid points. The algebraic equations are then solved in the discretized space by means of appropriate boundary conditions.

The generation of high-quality grids is a tedious task in CFD applications for geometrically intricate flow domains. The multi-block strategy for grid generation, available in the CFX-4 software, relies on a two-stage approach. The flow domain is first subdivided into small cuboidal regions called blocks. The final meshing into cells proceeds on a block-by-block basis, while maintaining appropriate matching conditions at the boundaries of contiguous blocks. Unmatched grids are allowed in CFX-4, but they were not used in this analysis to avoid possible interpolation errors.

3.1 Grid 1: Grid with Part of Core

The first of the two grids for the CFD simulations of the IRF chimney is shown in Figure 2.

The flow domain includes the chimney structure, the outlet pipes and parts of the two core segments. Each of the eight control rods is also modelled. The guide frames are treated as a solid regime, and the flow tubes for 18-element bundles are simulated as normal pipes. The domain for the outlet pipes extends farther than is shown in Figure 1.

Figure 2 shows that they extend up to the ends of the 90° bends to reduce the influence of the pipe outflow boundary conditions on the flow inside the chimney. The FN fuel sites are not simulated directly. Instead, the flows from the FN fuel sites are treated as boundary conditions imposed over small openings on the side walls of the chimney. A small portion of the core is also represented in this grid. This part of the core is divided into two layers. The upper one is treated as an isotropic porous medium to simulate the effects of the core on the velocity profile at the entrance to the chimney. Because boundary conditions cannot be specified directly on the boundary of the porous medium, the lower layer of the core is modelled as an empty tube.

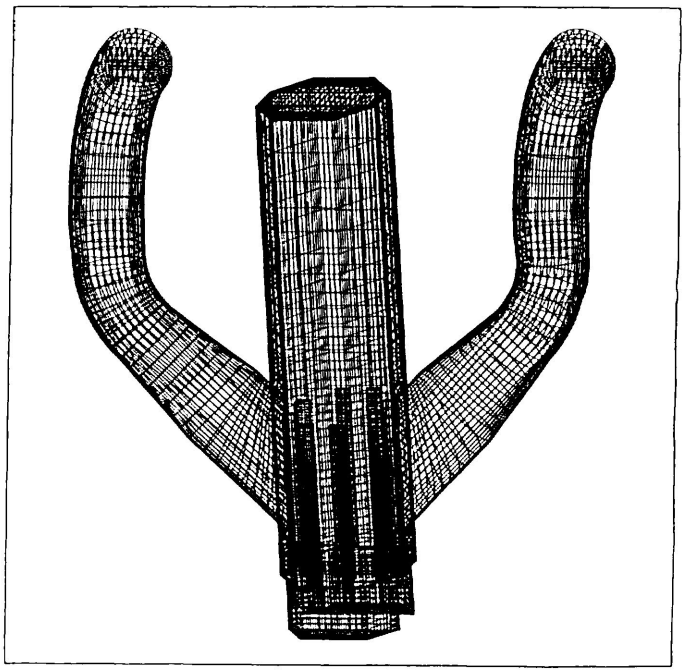

Fig.2 Grid 1 with a Tilted View

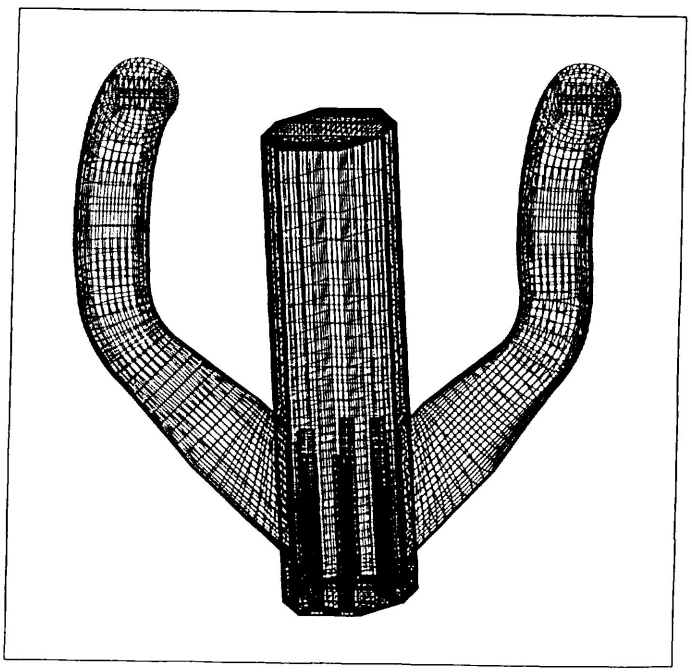

Fig.3 Grid 2 with a Tilted View

The grid is built using 1190 blocks, and it contains almost 190 000 cells. The non-uniform node distribution is effected by invoking the geometric-progression in CFX-4. A denser distribution is used near walls and in regions where large variations of velocities or temperature are anticipated. The flow from the core is set as the inlet-type boundary condition;

flows through the chimney top, FN sites, and outlet pipes are modelled as mass-flow-type boundary conditions.

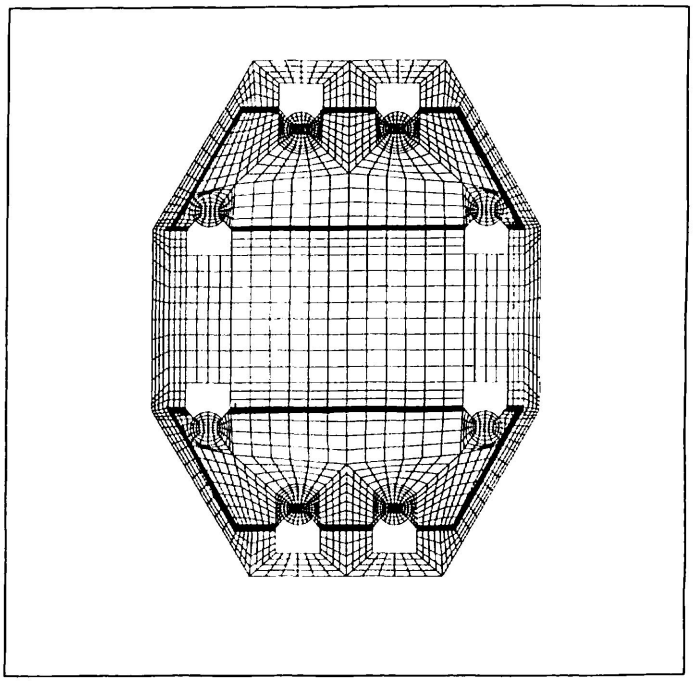

Fig.4 The Bottom Plane of Grid 2

3.2 Grid 2: Grid Without Core

In grid 1 the porous medium model is used to represent the core to account for its effects on the velocity distribution. In this approach, when the flow enters the chimney from the core, the velocity has to be abruptly reduced by about 42%, to satisfy the principle of mass conservation. The simulation using grid 1 does not model the momentum of the core jets properly. To alleviate this shortcoming, grid 2 was generated. In this grid, the porous-medium model of the core was removed, and the velocity is specified directly over the bottom plane of the chimney, to satisfy momentum boundary conditions.

The mass-flow-type boundary conditions are defined in the same way as they were defined in grid 1. This grid, shown in Figure 3, has 1000 blocks and 170 000 cells.

Figure 4 depicts the bottom plane of the chimney. The two regions indicated by bold boundaries represent the area where the core flow enters the chimney.

4. MATHEMATICAL MODELS AND BOUNDARY CONDITIONS

In this section, the details of the mathematical models underlying all simulations— together with boundary conditions, and modelling simplifications— are outlined.

4.1 Simplifying Assumptions

The following simplifying assumptions were made about the physical processes in the IRF chimney:

1. The light water coolant is a Newtonian, incompressible fluid, and the flow is steady and turbulent. All fluid properties are based on the reference (pool) temperature of $T = 35^{0}C$.

2. The effects of the buoyancy on the flow pattern in the chimney are negligible. The ratio of characteristic buoyancy to inertia forces is defined as the ratio of Grashof number to the square of the Reynolds number, $\frac{Gr}{\mathrm{Re}^2} = \frac{\alpha\, g\, \Delta T D}{V^2}$, where α is the thermal expansion coefficient, g is the gravitational acceleration, ΔT is the characteristic temperature difference, D is the chimney diameter, and V is the characteristic velocity. In this study

$$\frac{Gr}{\mathrm{Re}^2} = \frac{3.398\times10^{-4}\times9.81\times20\times0.845}{7.18^2} = 0.0011$$

   The buoyant force is therefore much smaller than the driving inertia force, and hence buoyancy effects were not considered in any simulations.

3. The core was represented as an isotropic porous medium, assuming a constant porosity of $v = 0.58$, based on the ratio of flow area to the total area of the core. Because the most important effect resulting from this model was the reduction of average velocity entering the chimney, porous-medium resistance was not included inside the core.

4.2 Governing Equations

The time-average equations of continuity, momentum, and energy, written for steady-state, incompressible, turbulent flow, are

continuity:

$$\frac{\partial u_i}{\partial x_i} = 0 \qquad (1)$$

momentum:

$$\rho u_j \frac{\partial u_i}{\partial x_j} = F_i - \frac{\partial p}{\partial x_i} + \frac{\partial}{\partial x_j}\left[\ (\mu+\mu_t)\left(\frac{\partial u_i}{\partial x_j} + \frac{\partial u_j}{\partial x_i}\right)\ \right] \qquad (2)$$

energy:

$$\rho\ C_p u_j \frac{\partial T}{\partial x_j} = \frac{\partial}{\partial x_j}\left[(k_m + k_t) \frac{\partial T}{\partial x_j} \right] + Q_T \tag{3}$$

where:

u_i are the Cartesian components of the mean velocity;

F_i, ρ and μ are the volume force acting on the fluid, density, and molecular viscosity of the fluid, respectively;

μ_t is the turbulent (eddy) viscosity, depending on both the physical properties of the fluid and the properties of the flow. It generally changes from one position to another in steady-state problems;

T is the mean temperature of the fluid;

T_0 is the buoyancy reference temperature, and α is the coefficient of thermal expansion;

C_p is the heat capacity of the fluid at constant pressure;

k_m and k_t are the molecular and turbulent conductivities, respectively; and

Q_T is the source or sink of heat per unit volume.

These equations do not constitute a closed system, because the turbulent viscosity and conductivity are not constants, and are not known in advance. Turbulence models are used to close the system of mean flow and energy equations. These models simulate the effects of turbulence on the mean flow behaviour, leaving the details of the turbulence structure of the flow unresolved. A well-established turbulence model is the $k-\varepsilon$ model:

$$u_j \frac{\partial k}{\partial x_j} = \frac{\partial}{\partial x_j}\left(\frac{\mu + \mu_t}{\rho \sigma_k} \frac{\partial k}{\partial x_j}\right) + G - \varepsilon \tag{4}$$

$$u_j \frac{\partial \varepsilon}{\partial x_j} = \frac{\partial}{\partial x_j}\left(\frac{\mu + \mu_t}{\rho \sigma_\varepsilon} \frac{\partial \varepsilon}{\partial x_j}\right) + \frac{C_1 \varepsilon G - C_2 \varepsilon^2}{k} \tag{5}$$

where:

k is the turbulent kinetic energy, i.e. $k = \frac{1}{2}\left(\overline{(u_1')^2} + \overline{(u_2')^2} + \overline{(u_3')^2}\right)$,

ε is the dissipation rate of turbulent kinetic energy,

G is the turbulence generation term, and

C_1, C_2, σ_k, σ_ε are empirical constants.

With k and ε known, the eddy (or turbulent) viscosity and turbulent conductivity can be calculated as $\mu_t = \rho C_\mu \frac{k^2}{\varepsilon}$ and $k_t = \frac{\mu_t}{\sigma_T}$,where C_μ=0.09 and σ_T=0.9.

The finite-volume methodology is adopted to discretize these governing equations in CFX-4. The most attractive feature of this methodology is that the conservation of transported quantities (mass, momentum, and energy) is satisfied over any individual cell, and hence over the whole computational domain.

The convergence criteria for the numerical solution of the governing equations (1) to (5) are set to 0.5% mass residual for the velocity field and 1% enthalpy residual for the temperature calculation.

4.3 Boundary Conditions

Three kinds of boundary conditions are specified, as listed below:

4.3.1 Inlet-Type Boundary Conditions. The flow entering the core is specified as the inlet-type boundary condition. With this boundary condition, all relevant variables (velocity, turbulence quantities and temperature) are fixed. The velocity and temperature were obtained from CATHENA [3] calculations and the design specifications. The turbulence quantities were calculated as follows:

$$k = 0.004 V^2 \quad and \quad \varepsilon = k^{1.5} / (0.3d) \tag{6}$$

where V is the velocity at the inlet, and d is the hydraulic diameter.

4.3.2 Mass-Flow-Type Boundary Conditions. The flow rates through the top of the chimney, the two outlet pipes, and the four FN tubes are specified by imposing mass-flow-type boundary conditions. With these boundary conditions, the net mass flow rate is fixed and the relevant variables are calculated as if it were a fully developed flow.

4.3.3 Wall-type Boundary Conditions. The velocities are fixed at zero along all the walls within the chimney structure. All the walls are assumed to be adiabatic.

As the velocity and temperature can change very rapidly near the walls in turbulent flows, it could require a very fine grid to resolve their variations in the near-wall zones. This would be prohibitively costly, and hence in the CFX-4 application the near-wall zone is solved by using "wall functions" [2]. In the work reported here, the main interest is to account for the wall friction. This is done with sufficient accuracy using the "wall-function" method.

5. RESULTS AND DISCUSSION

Three cases were run using grids 1 and 2. Velocity, turbulence quantities, and temperature were fixed at the main core exit for all the simulations (inlet-type boundary conditions). The flows through the FN tubes, chimney top, and out of the discharge tubes were treated as mass-flow-type boundary conditions. The relative mass flow rates are specified on these boundaries as -0.14 m, -0.15 m, and 1.29 m, respectively, with m denoting the mass-flow rate through the core. The negative sign indicates that flow is into the chimney, and the positive sign means flow out of chimney. These relative mass-flow rates remained fixed for all cases.

5.1 Case 1: Simulation with Grid 1

In the simulation using grid 1, the vertical velocity W = 3.16 m/s and temperature $T = 47\,^{0}C$ were specified on the core inlet boundary. The turbulence quantities on this boundary were calculated using Equation (6). The calculated velocity field on the vertical mid-plane Y = 0 is shown in Figure 5 (scale 1 cm : 2.24 m/s). It can be seen that the velocity is symmetric about the chimney axis.
The maximum velocity occurs near the two openings to the discharge tubes. There are two recirculation zones near the

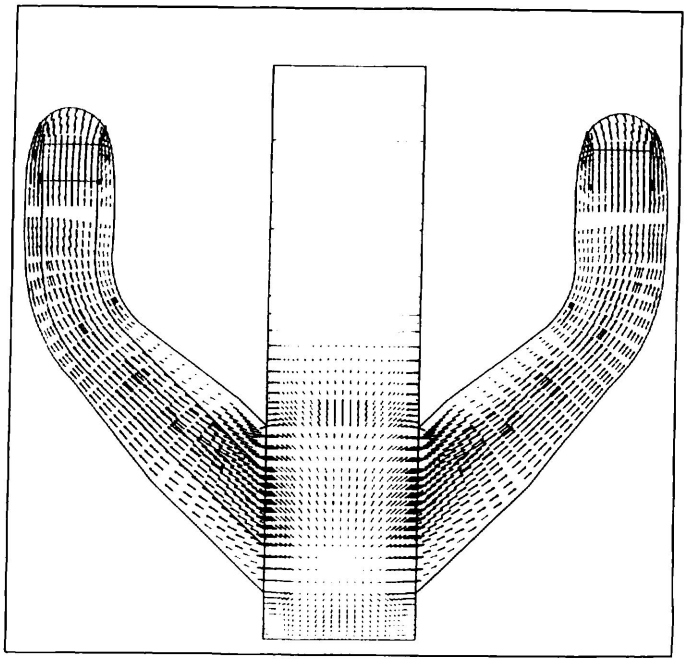

Fig. 5 Velocity Field in Y=0 Plane for Case 1

corners of the chimney, generated by the core jets. Some core flows certainly pass the suction part. The highest position reached by the core jets is at the centre of the chimney, 1.44 m from the chimney bottom. This position was established by drawing the contours of vertical velocity W at various Z = const planes. The pressure distribution across the mid-plane is depicted in Figure 6. The lowest pressure was predicted at the upside of the junction between the discharge tubes and the chimney. The maximum pressure difference inside the chimney is about 30 kPa.

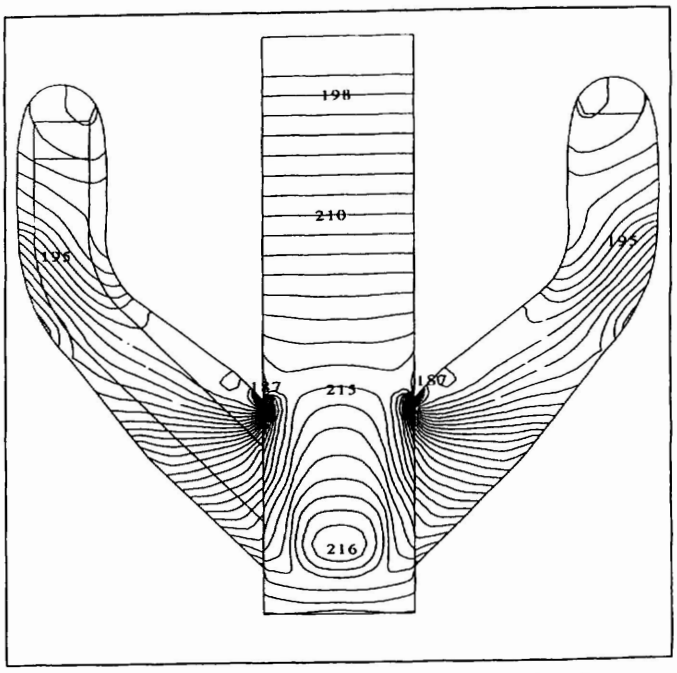

Fig.6 Pressure Distribution in Y=0 Plane for Case 1

The temperature distribution in the mid-plane is illustrated in Figure 7. It is also symmetric. The lowest temperatures are predicted, as expected, at the upper part of the chimney, on account of the cool water entering the chimney top from the pool. The temperature for flow from the FN tubes is 55^0C, and 47^0C for the core flow. When the flow reaches the exit of the discharge tube, it is very well mixed. The flow has a uniform temperature of about 47.5^0C.

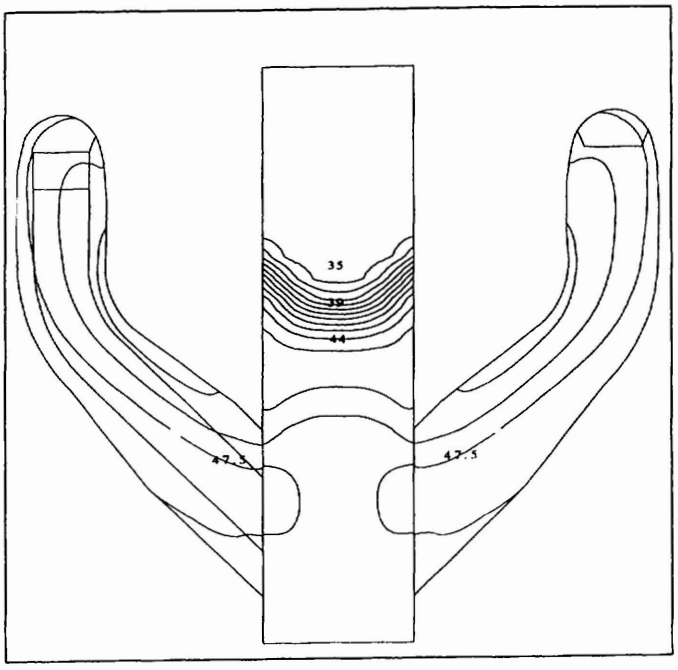

Fig.7 Temperature Distribution in Y=0 Plane for Case 1

5.2 Case 2: Simulation with Grid 2 Assuming a Uniform Inlet Velocity

As discussed in Section 3.2, the simulation using grid 1 did not accurately represent the momentum of the core jets entering the chimney because of the porous-medium model. In this simulation, grid 2 was used, and thus the core was completely removed. The inlet boundary is set directly at the bottom of the chimney. The CATHENA results indicate that the maximum coolant velocities inside the 18-element and 36-element bundles are assumed to be 9.33 m/s and 7.18 m/s, respectively. Thus the averaged maximum velocity in the main core is calculated to be

$$V = \frac{V_{18} \times A_{18} + V_{36} \times A_{36}}{A_{18} + A_{36}} = 7.55 \text{ m/s}$$

In this study, a uniform velocity distribution of $W = 7.55$ m/s was specified at the inlet boundary at the chimney bottom, to approximate the maximum momentum of the jets. This simulation results in a maximum flow rate through the chimney. This extreme case was deemed to be meaningful because our basic concern was whether the core jets would leak out of the chimney. The real situation must be bounded by cases 1 and 2.

The velocity field and pressure distributions in mid-plane were still predicted to be symmetric about the chimney axis. However, on average, the magnitudes of the velocities were larger than case 1. In both cases 1 and 2, the pressures at the upper part of the chimney were almost the same, but the minimum pressure in case 2 was much smaller than in case 1. Examination of the contours of vertical velocity at different Z = const planes indicates that the highest position reached by the core jets was 1.73 m from chimney bottom, and near the chimney side walls, rather than at the chimney centre. This finding means that the flow patterns changed significantly when the core was removed and a uniform velocity of larger magnitude was specified directly at the bottom of the chimney.

The temperature field was also predicted to be symmetric about the chimney axis. The temperatures at the exits of the discharge tubes were found to have uniform distribution.

5.3 Simulation with Grid 2 Assuming a Non-uniform Inlet Velocity

In case 2, a uniform velocity of 7.55 m/s was set at the inlet boundary, despite the fact that CATHENA results indicate that the velocity at the main core outlet is not uniform. In case 3, the simulation was performed using grid 2, but a non-uniform velocity profile was specified on the inlet boundary at the chimney bottom (see Figure 5). A uniform vertical velocity $W = 9.33$ m/s was specified inside the 18-element bundles, and $W = 7.18$ m/s was assumed for the rest of the core.

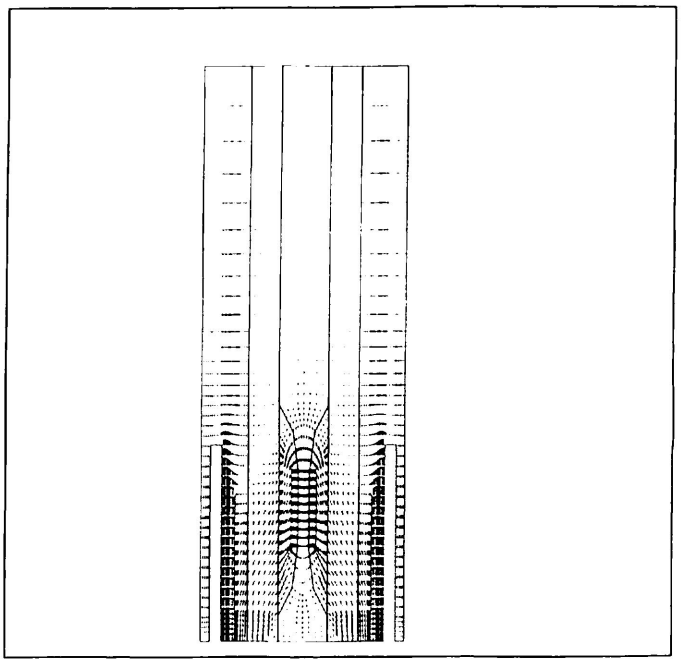

Fig.8 Velocity Field in X=0.084 m Plane for Case 3

Again, the velocities, pressure, and temperature in the mid-plane Y = 0 were all symmetric about the chimney axis. However, the maximum velocity in this plane was predicted to be smaller than that in case 2, and the temperature distribution at the elevation corresponding to the jet extinction is quite different from that in case 2. The pressure ranges are very close for both cases 2 and 3.

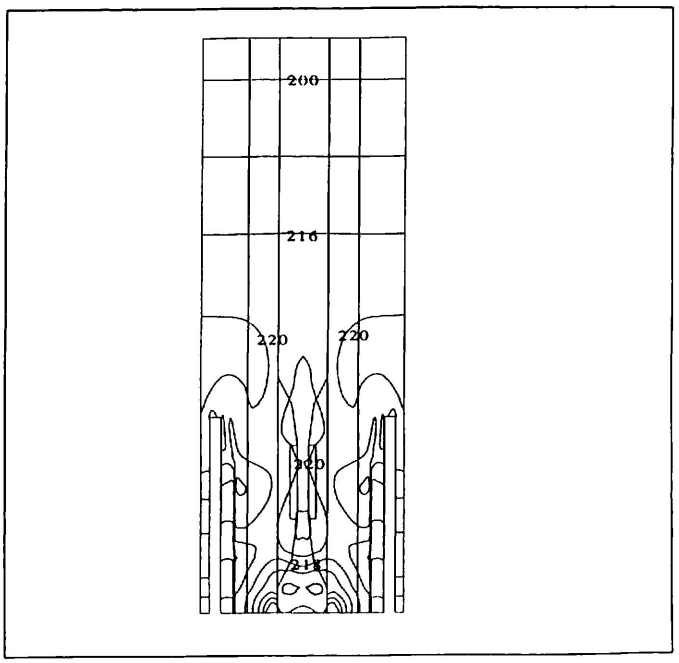

Fig.9 Pressure Distribution in X=0.084 m Plane for Case 3

Figures 8, 9, and 10 show the velocity, pressure, and temperature distributions in the

plane of X = 0.084 m. This plane cuts through the centre of two flow tubes, just left of the chimney axis (see Figure 4). The asymmetric arrangement of the outlet pipes had no influence on the flow patterns inside the chimney. Figure 8 (scale 1 cm : 3.80 m/s) clearly shows that the 2 jets from the flow tubes for 18-element bundles die away very quickly. The temperature distribution, shown in Figure 10, indicates that the highest position the core jets can reach is at the centre. The maximum elevation reached by the core jets was predicted to be 1.47 m from the chimney bottom.

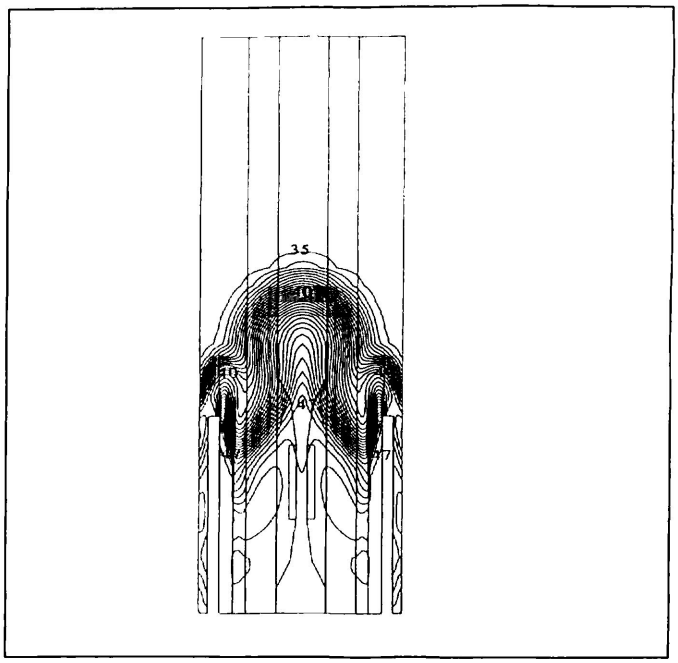

Fig.10 Temperature Distribution in X=0.084m Plane for Case 3

6. CONCLUSIONS

A numerical investigation of the flow and heat transfer in the IRF chimney was conducted using the commercial CFD software, CFX-4. The assessment of the flow and temperature patterns was based on three-dimensional simulations, using a realistic representation of chimney geometry. The studies indicate that the current design of the IRF chimney is adequate to contain core jets, and thus radioactive particles will be confined to the chimney.

The results of this study show that the flow patterns inside the chimney are symmetric about the X-Z and Y-Z planes. The predicted maximum elevations reached by the core jets are between 1.44 ~ 1.73 m from the bottom of the chimney. This distance was found to be determined predominately by the ratio of the mass-flow rate entering the chimney top and leaving the core. The velocity profile of the core outflow also influences the flow patterns inside the chimney.

The temperature distributions are also found to be symmetric about the X-Z and Y-Z planes. The flow from the core and FN tubes was predicted to undergo a rapid mixing in the outlet pipes, yielding uniform temperature at their exits.

ACKNOWLEDGEMENT

The authors are grateful to W. E. Bishop for useful suggestions during the course of this work.

REFERENCES

[1] Lee A. G., Bishop W. E., Gillespie G. E. and Zeng Y., "Progress in Developing the Concept for the Irradiation Research Facility", AECL Report, AECL-11508, 1996 April.

[2] CFX4.1 User Guide, AEA Technology, Computational Fluid Dynamics Services, 1995 October.

[3] Hanna, B. N., "CATHENA: A Thermalhydraulic Code for CANDU Analysis", Nuclear Engineering and Design, 1998 March, 180 (2), pp. 113-131.